Second-harmonic generation in reflection and diffraction by a GaAs photonic-crystal waveguide

Andrea Marco Malvezzi

Istituto Nazionale per la Fisica della Materia, and Dipartimento di Elettronica, Università degli Studi di Pavia, Via Ferrata 1, I-27100 Pavia, Italy

Francesco Cattaneo, Gabriele Vecchi, Matteo Falasconi, Giorgio Guizzetti, and Lucio Claudio Andreani

Istituto Nazionale per la Fisica della Materia, and Dipartimento di Fisica "A. Volta," Università degli Studi di Pavia, Via Bassi 6, I-27100 Pavia, Italy

Filippo Romanato, Luca Businaro, and Enzo Di Fabrizio

National Nanotechnology Laboratory, TASC–Istituto Nazionale per la Fisica della Materia Nanolithography Beamline at Elettra Synchrotron Light Source, S.S14 Km 163.5, I-34012 Basovizza-Trieste, Italy

Adriana Passaseo and Massimo De Vittorio

National Nanotechnology Laboratory, Istituto Nazionale per la Fisica della Materia, and Dipartimento di Ingegneria dell'Innovazione, Università degli Studi di Lecce, via per Arnesano, I-73100 Lecce, Italy

Received November 30 2001; revised manuscript received March 11, 2002

Nonlinear reflection and diffraction measurements have been performed on a GaAs/AlGaAs photonic-crystal waveguide patterned with a square lattice: The basis in the two-dimensional unit cell consists of rings of air in the dielectric matrix. The measured angles of diffracted second-harmonic beams agree with those predicted for nonlinear diffraction conditions. Results for second-harmonic intensities as a function of incidence angle, polarization, and pump wavelength show that the reflected second-harmonic signal is dominated by the crystalline symmetry of GaAs, whereas nonlinear diffraction is determined by the photonic-crystal structure.

OCIS codes: 190.4720, 190.4400, 190.2620, 190.4390.

1. INTRODUCTION

Since the first prediction of nonlinear diffraction in spatially modulated systems,[1] the subject of second-harmonic generation (SHG) in diffraction from nonlinear gratings has received much attention both experimentally and theoretically.[2–16] A second-harmonic (SH) beam generated by the nonlinear material and diffracted by the grating occurs at directions given by nonlinear diffraction conditions (if the material is rough, diffracted SHG occurs also in a diffusion cone[1]). The diffracted SH signal is obviously small for a shallow grating and increases with groove depth. Many papers[3–6] deal with one-dimensional metallic or metallodielectric gratings and with resonance effects related to surface plasmons; others[7–12] exploit SH diffraction by a monolayer grating on top of a centrosymmetric medium for the study of surface phenomena (adsorption, diffusion, etc.) without the need to consider effects of the substrate. Recently, nonlinear diffraction during in-plane propagation in two-dimensional (2-D) photonic crystals with spatially varying $\chi^{(2)}$ was predicted[17] and experimentally observed.[18]

One- and two-dimensional photonic-crystal slabs based on GaAs (Refs. 19 and 20) are well suited for SHG studies of reflection and diffraction because the second-order susceptibility of GaAs is large and photonic lattices at optical wavelengths can be defined and patterned deeply into the samples by lithography and etching. The main difference between a photonic crystal and a conventional grating is that in the former the etch depth is large, leading to strong efficiencies for *linear* diffraction.[21,22] As is well known, for well-defined photonic modes with reasonably low propagation losses, the photonic pattern must be impressed in a planar waveguide, and the average dielectric constant of the claddings must be lower than that of the core layer after the patterning: For symmetric GaAs/AlGaAs or asymmetric air/GaAs/AlGaAs photonic-crystal slabs, this means that the lower cladding has to be etched to a certain depth.

In this paper, we report on SHG measurements of reflection and diffraction from an air/GaAs/$Al_xGa_{1-x}As$ photonic-crystal waveguide patterned deeply with a 2-D square lattice of air rings. The lattice has a low air fraction (~12%) and an etch depth of more than 1μm: Indeed, linear reflectance measurements at various angles on this sample[23] showed narrow resonances, which point to the existence of low-loss photonic modes, as were first shown in triangular lattices of holes in the research reported in Ref. 24. We detected the diffracted SH signal

from a waveguide excited with a Ti:sapphire laser and verified the nonlinear diffraction rules by performing experiments at various angles of incidence. Also, we measured the reflected and the diffracted intensities as functions of the wavelength (in the spectral range allowed by tuning of the Ti:sapphire oscillator) and of the polarization of the incident beam. These measurements, when compared with reflection SHG on the unpatterned waveguide area, point to high diffraction intensities and to polarization properties that are characteristic of the photonic-crystal waveguide.

This paper is organized as follows: We first give a description of the sample and of the experimental setup and illustrate the nonlinear diffraction rules for the crystal structure and experimental geometry that we have chosen. We then present and discuss the experimental results for nonlinear reflection and diffraction. Section 5 contains concluding remarks.

2. EXPERIMENTAL

The waveguide investigated in this study was grown by metal–organic chemical vapor deposition upon a (100) semi-insulating GaAs substrate. The structure consists of a 200-nm GaAs buffer layer, a 1500-nm $Al_{0.25}Ga_{0.75}As$ lower cladding, and a 500-nm GaAs core layer (nominally undoped): Thus the upper layer is GaAs and the air/GaAs/$Al_{0.25}Ga_{0.75}As$ waveguide is asymmetric. We patterned the waveguide by x-ray lithography, followed by reactive-ion etching. The mask for x-ray lithography was generated by electron-beam lithography on a 4 mm $\times$ 4 mm area, and it consisted of a square lattice of square holes (282 nm on a side) rotated by 45° with respect to the axes of the lattice. Proximity x-ray lithography performed at the LILIT beam line at the ELETTRA Synchrotron (Trieste, Italy) was employed to transfer the patterning to the sample surface. A diffraction effect in x-ray lithography, controlled by the distance between the mask and the stepper, resulted in partial filling of the air pillars and in a reduction of the air fraction. Reactive-ion etching with $SiCl_4$ was then performed to pattern the photonic lattice deeply into the waveguide. The etch depth was more than 1 μm. Two scanning electron micrographs of the sample are shown in Fig. 1. The Bravais lattice is a 2-D square lattice with lattice constant of $a = 500$ nm, and the basis within the unit cell consists of a ring of air in the dielectric matrix. The air fraction of the photonic lattice is approximately 12%. Note that the orientation of the mask was chosen in such a way that the square axes of the photonic lattices coincide (within a small uncertainty) with the crystallographic axis [110] of GaAs: The [100] axis of the microscopic lattice (which determines the symmetry properties of the $\chi^{(2)}$ tensor) and the [10] axis of the photonic lattice (which produces the diffractive effects) are rotated by 45° with respect to each other.

In Fig. 2, we show the linear reflectance of the sample at various angles of incidence for *s*-polarized light incident along the $\Gamma-M$ orientation.[23,24] Complex oscillations that resulted from Fabry–Perot interference in the waveguide structure are apparent. At 0.6–1 eV, narrow resonant structures with a well-defined angular dispersion can be seen. They are due to the excitation of photonic modes of the waveguide that were coupled to the incoming field by the patterning. The energy positions of these modes are indicated on the $\theta = 5°$ and the $\theta = 60°$ curves by vertical bars. Figure 2 shows that the sample behaved as a photonic-crystal slab with well-defined photonic modes: It also shows that the energy window in which these modes were resonantly coupled to an external field was 0.6–1 eV. For higher energies no structures associated with photonic modes were observed. Similar results were obtained for other polarizations and sample orientations. The Fabry–Perot oscillations were modeled to be consistent with the 1-μm etched depth of the photonic structures.[23]

The source of excitation for SHG measurements is a Ti:sapphire laser system that provides pulses of an $\approx$130-fs duration at an 80-MHz repetition rate centered at wavelengths of 750–840 nm, with an average power on sample of as much as 150 mW. The ultrashort-pulsed laser was used here to provide a sufficiently high intensity for obtaining a detectable SH signal, while minimizing the thermal load to the sample. Pulses were focused to a 40–50-μm diameter with a 20-cm focal-length lens onto

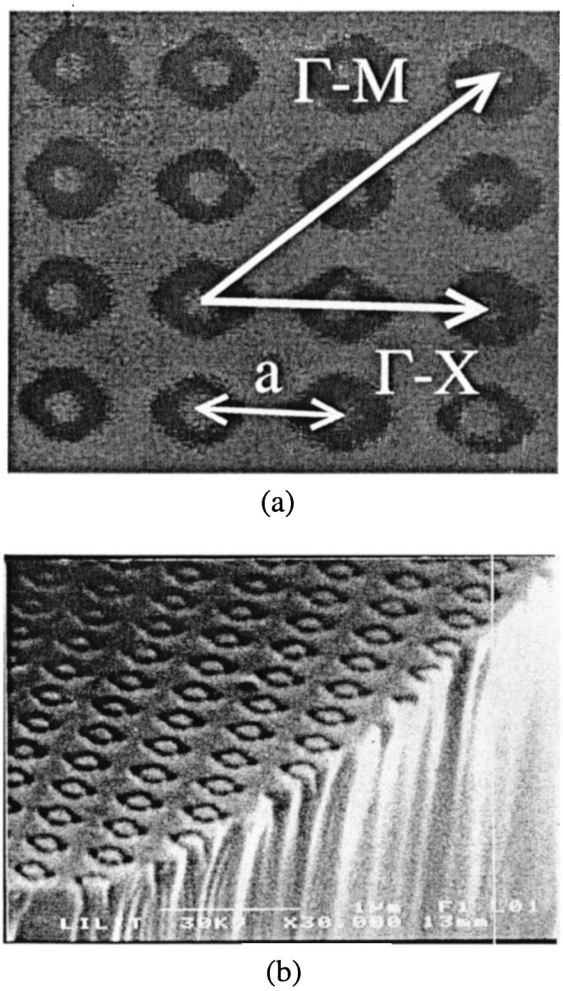

Fig. 1. Scanning electron micrographs of the sample studied in the research reported here. (a) Front view, (b) cross section showing vertical air structures. The lattice constant of the square Bravais lattice is $a = 500$ nm.

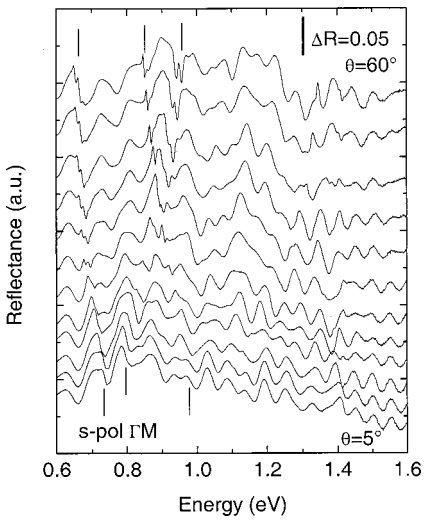

Fig. 2. Linear variable-angle reflectance for *s*-polarized light (s-pol) incident in the $\Gamma-M$ direction. The angle of incidence varies from 5° to 60°, in steps of 5°. The curves are shifted vertically for clarity. The vertical bars denote the energy positions of the photonic resonances for $\theta = 5°$ and $\theta = 60°$.

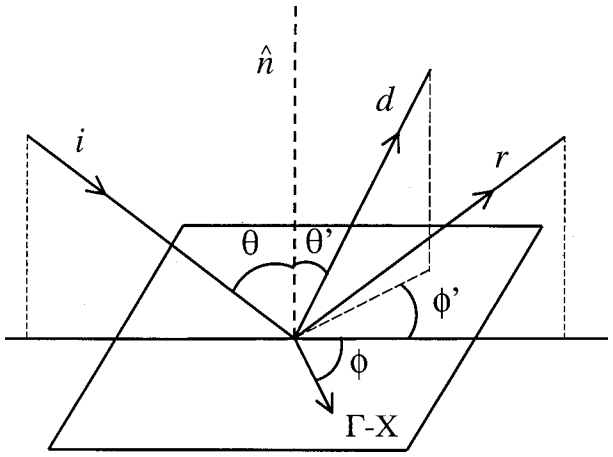

Fig. 3. Experimental geometry for SHG at the sample. The incident (i), reflected (r), and diffracted (d) wave directions are represented by thick lines. n is the normal to the sample surface, and the relevant angles are indicated.

the sample after filtering and intensity and polarization controls. The SH radiation was collected by an optical fiber (400-μm core diameter) and delivered in front of a cooled photomultiplier after passing through a combination of color filters plus a wideband interference filter that rejected the radiation at the pump frequency. No polarization selection of the SH signal was implemented. The optical fiber was of UV–visible type, transmitting more than 95% of the radiation at 400 nm.

The geometry of the optical layout is sketched in Fig. 3, where the notation for the angles involved in the experiment is also shown. It includes the angle of incidence θ of the pump radiation, angle ϕ formed by the $\Gamma-X$ direction of the photonic crystal to the plane of incidence, polar diffraction angle θ' measured from the normal n to the sample, and the azimuthal angle ϕ' of the diffracted beam (also measured from the plane of incidence). Of these four angles all are variable in the experimental setup except ϕ', which we kept fixed at 0° or 180°. Thus, only in-plane diffraction beams (forward and backward) were being detected, whereas θ' and ϕ were remotely controlled in 0.225°/step increments. Optical alignment of the setup requires that a set of translation stages for the azimuthal axis of rotation of the sample (defining ϕ) and its polar axis of rotation (defining θ) cross at the laser focal spot on the sample surface. Moreover, the rotation of the optical fiber (defining the angle θ') has to share the same vertical axis of rotation.

The SH signal is detected with a light chopper, which modulates the pump radiation up to a few kilohertz. The photomultiplier signal is then recorded by an averaging oscilloscope, so the amplitude of the signal with respect to background is evaluated.

3. NONLINEAR DIFFRACTION CONDITIONS

For a given incidence angle and sample orientation a SH beam is generated in all directions that satisfies the following conditions:

$$\mathbf{k}_{\parallel}' = 2\mathbf{k}_{\parallel} + \mathbf{G}, \tag{1}$$

where $\mathbf{k}_{\parallel}$ ($\mathbf{k}_{\parallel}'$) is the parallel wave vector of the incident (SH) beam and $\mathbf{G}$ is a reciprocal lattice vector of the photonic lattice. For $\mathbf{G} = 0$, we have the usual SHG on reflection. One can view the diffracted SH beam [$G \neq 0$ in

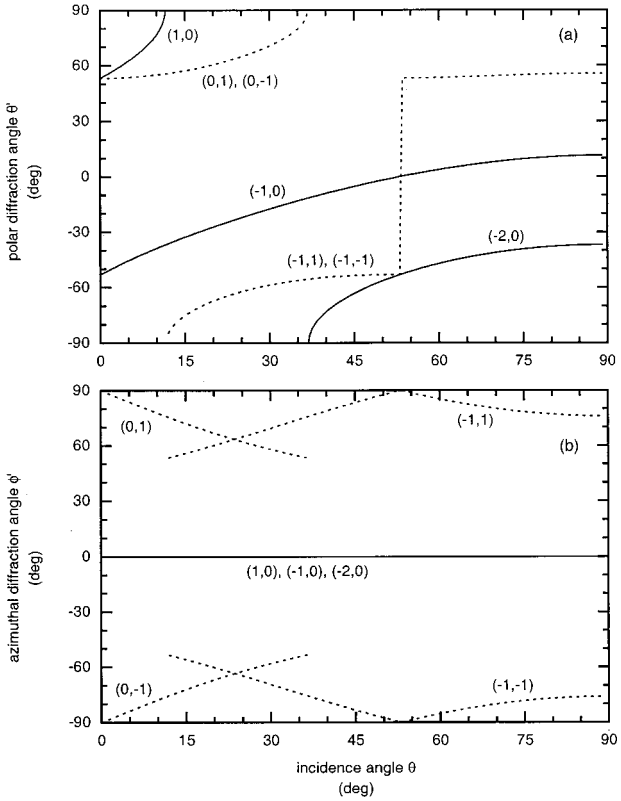

Fig. 4. Nonlinear diffraction angles for light incident along the $\Gamma-X$ orientation of the photonic crystal, assuming that $\lambda = 800$ nm and $a = 500$ nm: (a) polar angle θ', (b) azimuthal angle ϕ'. Solid (dotted) curves, diffraction in the plane (out of the plane) of incidence. The integer numbers (n_1 and n_2) that label the diffraction order [Eqs. (2)] are indicated on each curve.

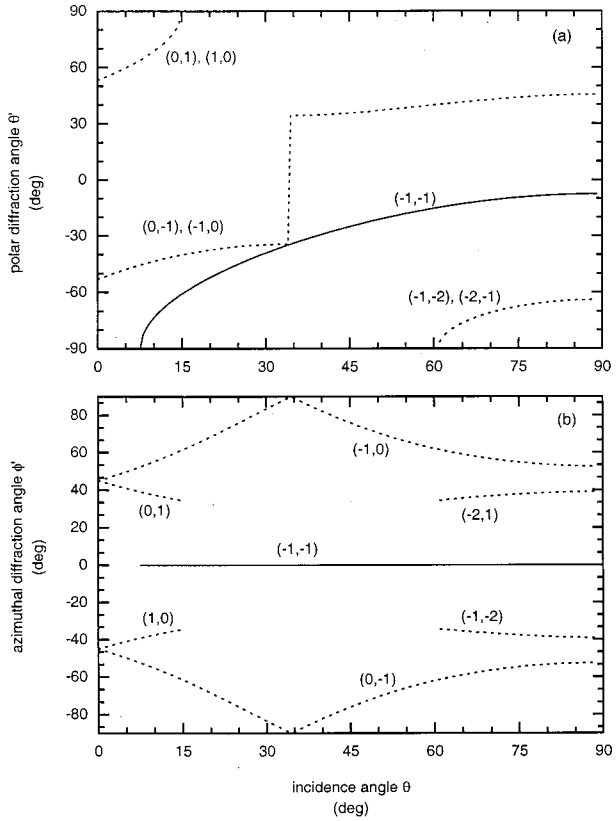

Fig. 5. Nonlinear diffraction angles for light incident along the Γ–M orientation of the photonic crystal, assuming that $\lambda = 800$ nm and $a = 500$ nm: (a) polar angle θ', (b) azimuthal angle ϕ'. Solid (dotted) curves, diffraction in the plane (out of the plane) of incidence. The integer numbers (n_1 and n_2) that label the diffraction order [Eqs. (2)] are indicated on each curve.

Eq. (1)] as being due to SHG on reflection followed by diffraction at the harmonic frequency or else as being due to diffraction at the pump frequency followed by SHG: The two processes are physically indistinguishable.

We now specify the nonlinear diffraction conditions by making reference to the experimental scheme and the angles shown in Fig. 3. The reciprocal lattice vectors can be expressed as $\mathbf{G} = (2\pi/a)(n_1\hat{\imath} + n_2\hat{\jmath})$, where $\hat{\imath}$ and $\hat{\jmath}$ are unit vectors along the [1, 0] and the [0, 1] axes of the photonic lattice and $n_1, n_2 = 0, \pm 1, \pm 2, \ldots$. Thus Eq. (1) becomes

$$\sin\theta' \cos(\phi' + \phi) = \sin\theta\cos\phi + n_1\frac{\lambda}{2a},$$

$$\sin\theta' \sin(\phi' + \phi) = \sin\theta\sin\phi + n_2\frac{\lambda}{2a}, \qquad (2)$$

where λ is the wavelength of the pump beam. It can be seen that Eqs. (2) follow from the analogous equations for linear diffraction with the replacement $\lambda \to \lambda/2$. The wavelength at the cutoff for nonlinear diffraction is double that in the analogous linear process: As a consequence, nonlinear diffraction can occur even when linear diffraction is forbidden.

In general, most diffracted beams lie out of the plane of incidence. Only for an incident beam along the Γ–X direction of the lattice ($\phi = 0°$) or along the Γ–M direction ($\phi = 45°$) are there diffracted beams in the plane of incidence. These are the only beams that are detected by our experimental setup. To illustrate the physical conditions implied by Eq. (1), in Fig. 4, we show the angles θ' and ϕ' of all SH diffracted beams for light incident along the Γ–X direction, and, in Fig. 5, we show similar results for the Γ–M orientation. We chose the ratio $\lambda/a = 1.6$, corresponding to a lattice constant of $a = 500$ nm and a pump wavelength of $\lambda = 800$ nm. Diffraction in the plane of incidence is indicated by solid curves; diffraction out of the plane is marked by dotted curves. We resolved the ambiguity in the definitions of θ' and ϕ' by imposing the condition that $-\pi/2 < \phi' < \pi/2$: In this way a positive (negative) θ' means that diffraction occurs in the forward (backward) half-space. [This choice produces the jumps in Figs. 4(a) and 5(a), which correspond to diffracted beams with an angle ϕ' passing through 90° that changes from the backward to the forward half-space.] The curves are marked by the integers (n_1 and n_2) of Eqs. (2), which label the diffraction order.

The following conclusions can be drawn from Figs. 4 and 5: For light incident along Γ–X and considering all angles of incidence, there are as many as three SH beams diffracted in the plane of incidence, one of which is in the forward direction [the (1, 0) curve] and the other two of which are in the backward direction [the (−1, 0) and (−2, 0) curves]. The (−1, 0) nonlinear diffraction occurs for all angles of incidence. The other four diffracted SH beams (dotted curves) are out of the plane of incidence. For light incident along Γ–M, there is only one in-plane diffracted beam [corresponding to (−1, −1)], which occurs for all incidence angles larger than approximately 8°, and the six other diffracted beams are out of the plane of incidence. In general, it can be seen that nonlinear diffraction occurs preferentially in the backward geometry.

4. RESULTS AND DISCUSSION

With the apparatus described above, we measured the SH signal generated by the photonic crystal by fixing the sample orientation and varying the angle θ or the wavelength of the excitation radiation. The pump intensity on the sample was measured before each data-taking session by use of a calibrated powermeter and a knife-edge scan of the laser spot at the sample position. We calculated the intensity of the resultant SH radiation absolutely by considering the geometry of the apparatus, the detector response, and the transmission of the optical fiber and of the filters used in the spectral interval considered. As is discussed below, the calibration was checked against the SH generated in reflection from bulk crystalline GaAs samples. The SH signals detected both in reflection and in diffraction follow a quadratic law in the input fluence. The nonlinear radiation appears to be spatially coincident with the pump in reflection.

The diffraction angles of the SH signal are shown in Fig. 6 relative to the angle of incidence θ of the pump for a wavelength of 814 nm. The SH diffracted signals were measured for both *s* and *p* polarizations of the incident radiation and for both the Γ–X [$\phi = 0°$, curve (−1, 0) of Fig. 4] and the Γ–M [$\phi = 45°$, curve (−1, −1) of Fig. 5] photonic-crystal orientations. In the Γ–X orientation a

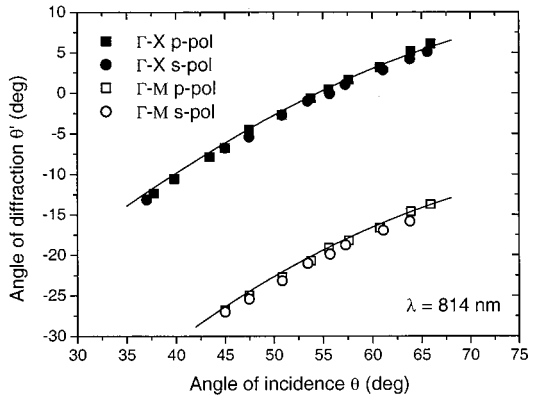

Fig. 6. Measured and calculated diffraction angles for light incident along the $\Gamma-X$ and the $\Gamma-M$ crystal orientations and for the two polarizations (s-pol and p-pol) of the pump beam as a function of the angle of incidence θ. The pump wavelength is 814 nm, and this value is also used for the theoretical curves.

further in-plane diffraction mode $(-2, 0)$ is predicted at a strongly negative $(-90° < \theta' < -35°)$ diffraction angle, which unfortunately could not be reached with the experimental setup. The theoretical SH diffraction curves with $\lambda = 814$ nm are also shown for the two cases. Agreement between the experimental results and the theoretical curves derived from Eqs. (1) and (2) is very good. The uncertainty of the incidence angles is approximately 1° and is the result of the alignment procedures both of the sample and of the incident laser beam. In the setup the optical fiber's angular position is not absolutely calibrated but is obtained by measurement of the position of the SH reflected signal. Thus the uncertainty in the angle of the SH reflected and diffracted beams is of the same order as the uncertainty in the incident angle.

For both reflected and diffracted SH measurements the nonlinear reflection and diffraction coefficients, defined as $R^{\mathrm{NL}} = I_R(2\omega)/I(\omega)^2$ and $D^{\mathrm{NL}} = I_D(2\omega)/I(\omega)^2$, respectively, were evaluated. In Fig. 7(a), nonlinear reflection coefficients R^{NL} measured at several angles of incidence θ are shown for various combinations of selected input polarization and photonic-crystal orientation at a pump wavelength of $\lambda = 814$ nm. These data are in good agreement with the theoretical calculation and the experimental results of the nonlinear reflection coefficient for a bulk nonpatterned (001) GaAs surface.[25–27] Indeed, the air-filling factor of the photonic crystal amounts to only 12% in this sample, leading to a nonlinear response that is close to that of bulk GaAs. A value of the order of $\sim 5 \times 10^{-24}$ m^2 W^{-1} for s polarization and the $\Gamma-X$ crystal orientation (which corresponds to light incident along the [110] crystallographic direction of GaAs) was obtained and compares favorably with that obtained from the measured value of $\chi^{(2)}$.[27] Similarly, consistent values were also obtained for the p polarization ($\sim 1 \times 10^{-22}$ m^2 W^{-1} with $\Gamma-M$ crystal orientation for both theoretical and experimental results). In fact, the SH reflected signal for incident p polarization is greater than for incident s polarization; for s polarization, $\Gamma-M$ signals (light incident along the [100] axis of GaAs) are lower than $\Gamma-X$ signals (light incident along the [110] axis of GaAs), whereas for p polarization the trend is the opposite. The occurrence of a large difference in the SH amplitudes on reflection with s and p input polarization is a useful test, in this case, of the mutual orientation of the GaAs crystal and the photonic lattice. Figure 7(a) therefore stresses the dominance, in nonlinear reflection, of the crystal symmetry of GaAs over the photonic lattice. The maximum values of R^{NL} that occur for $\theta \geq 50°$ for the p-polarized pump are due to increasing coupling of the input in proximity to the pseudo-Brewster angle of incidence. The inset in Fig. 7(a) shows the angular behavior of R^{NL} for p-polarized incident light calculated from the formula $R^{\mathrm{NL}} \propto |\epsilon_{2\omega}(\theta)\chi^{(2)}\epsilon_{\omega}(\theta)\epsilon_{\omega}(\theta)|^2$, where ϵ_{ω} ($\epsilon_{2\omega}$) is the linear (nonlinear) Fresnel factor[25] evaluated at the angle of incidence: This formula applies to SH reflection from a semi-infinite medium. The calculated curves are very similar to the measured ones, showing that neither the waveguide structure nor the patterning with low air fraction appreciably alters the angular dependence of the nonlinear reflection coefficient.

The nonlinear response determined by the photonic-crystal structure emerges instead from the study of the nonlinear diffraction coefficients. These are shown in Fig. 7(b) as a function of incident angle θ for $\lambda = 814$ nm pump wavelength, again for incident p and s polarization and for the two photonic-crystal orientations. First, we can observe that nonlinear diffracted coefficient data with s polarization are comparable with R^{NL} results for the same polarization, and this points to the importance of the diffraction process for this polarization. In

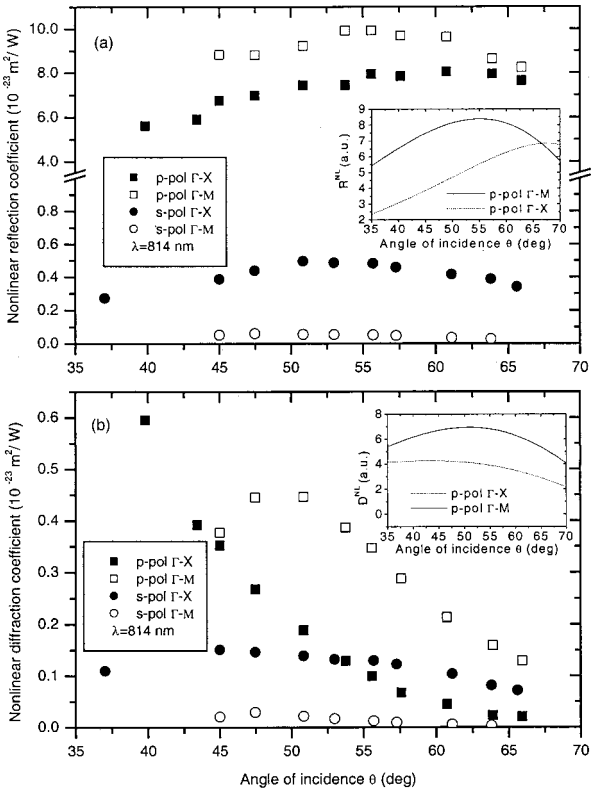

Fig. 7. Nonlinear (a) reflection and (b) diffraction coefficients as a function of angle of incidence for a pump wavelength of $\lambda = 814$ nm, for the crystal orientations and input polarizations (p-pol and s-pol) considered. Note the break in the vertical scale in (a). Insets, results of an approximate theoretical model (see text).

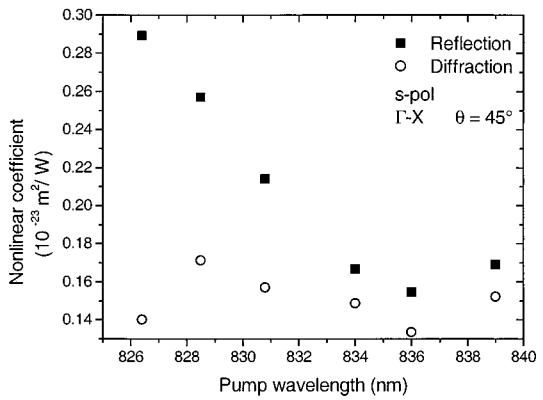

Fig. 8. Nonlinear reflection and diffraction coefficients as a function of pump wavelength for the $\Gamma-X$ sample orientation, angle of incidence $\theta = 45°$, and *s* polarization (s-pol).

addition to the angular dependence, it is interesting to compare the values of the coefficients in this *s*-polarization case. The diffraction efficiency $\eta = D^{\mathrm{NL}}/(D^{\mathrm{NL}} + R^{\mathrm{NL}})$ is of the order of 30% for both photonic-crystal orientations, indicating that a consistent fraction of the SH power is diverted by the photonic-crystal structure into the diffraction mode. (If nonlinear diffraction into all modes, including those out of the plane of incidence, were considered, the value of the diffraction efficiency would be even higher.) A distinctive indication of a photonic crystal is the θ dependence shown in the case of *p* polarization, which is characteristic of a macroscopic structure superimposed upon a GaAs substrate. In contrast to the behavior of nonlinear reflection, the nonlinear diffraction coefficient for *p* polarization has a decreasing behavior with angle of incidence in the $\Gamma-X$ orientation, whereas a maximum near 50° is measured for the $\Gamma-M$ photonic orientation. In an attempt to interpret the measured diffraction curves, we calculated the angular dependence of the nonlinear diffraction coefficient from the formula $D^{\mathrm{NL}} \propto |\varepsilon_{2\omega}(\theta')\chi^{(2)}\varepsilon_{\omega}(\theta)\varepsilon_{\omega}(\theta)|^2$, where now the nonlinear Fresnel factor $\varepsilon_{2\omega}$ was calculated at the diffraction angle θ'. This expression is exact in the case of shallow nonlinear gratings[8–11] for which the spatial variation of the linear susceptibility has a negligible effect and SH diffraction originates only from a modulation of $\chi^{(2)}$: In the present case, both linear and nonlinear susceptibilities are spatially modulated in the whole waveguide structure, and the theory of nonlinear diffraction is considerably more complex. The D^{NL} curves that arise from the formulas above are shown in the inset of Fig. 7(b), again for *p* polarization and for the two crystal orientations, and show striking similarities to the corresponding experimental curves. In particular, the maximum of D^{NL} for an incidence angle of $\theta \approx 50°$ for *p* polarization and $\Gamma-M$ orientation is reproduced. This maximum arises from the combined effects of the pseudo-Brewster angle [expressed by the Fresnel factor $\varepsilon_{\omega}(\theta)$ and also affecting the nonlinear reflection] and of the nonlinear Fresnel factor $\varepsilon_{2\omega}(\theta')$ at the diffraction angles θ' shown in Fig. 6. The remaining differences from the measured angular dependences of D^{NL} can be attributed to the waveguide structure and to the resultant Fabry–Perot oscillations.

In Fig. 8, we show the measured nonlinear reflection and diffraction coefficients as a function of the pump wavelength for *s* polarization and an incidence angle of $\theta = 45°$ with $\Gamma-X$ crystal orientation. These data further emphasize the fact that nonlinear diffraction by the photonic-crystal structure has completely different properties from nonlinear reflection. Indeed, a change of a factor of approximately 2 in R^{NL} is observed when the pump wavelength is changed from 826 to 839 nm, whereas an almost constant behavior of D^{NL} is observed. Comparing with the linear reflectance curves of Fig. 2, we see that SH measurements are made in a frequency region where no photonic mode of the patterned waveguide is observed but where pronounced Fabry–Perot oscillations still remain. Thus any theory of nonlinear reflection and diffraction must take into account the patterned waveguide structure with full modulation of linear and nonlinear optical susceptibilities in three dimensions.

5. CONCLUSIONS

Second-harmonic diffraction from a GaAs/AlGaAs photonic-crystal waveguide with a square lattice has been measured at the wavelengths of a Ti:sapphire laser. The angles of diffracted SH beams agree well with those predicted by nonlinear diffraction conditions. Results for reflected SH intensities are close to those for a (001) GaAs crystal surface, with the 45° rotation between the square photonic lattice and the [100] crystallographic axis of GaAs taken into account. This is so because of the low air fraction of the photonic crystal and shows that the reflected SH signal is essentially determined by the microscopic crystalline symmetry of GaAs rather than by the photonic lattice. The dependence of diffracted SH intensities on incidence angle, input polarization, and pump wavelength, however, is different from that of SH reflection owing to the properties of the photonic lattice. The diffraction-to-reflection ratio is large and points to the importance of nonlinear diffraction in photonic crystals, just as for the analogous linear phenomenon. Theoretical calculations of the diffraction intensities are in progress and will contribute to a detailed understanding of the nonlinear process.

ACKNOWLEDGMENTS

This study was supported in part by the Istituto Nazionale per la Fisica della Materia (INFM) PAIS 2001 project "2DPHOCRY" and by the INFM Femtosecond Lab. The authors are grateful to Y. Chen and D. Peyrade for performing part of the processing and to M. Galli and M. Patrini for linear reflectance measurements of the sample.

REFERENCES

1. I. Freund, "Nonlinear diffraction," Phys. Rev. Lett. **21**, 1404–1406 (1968).
2. R. Reinisch and M. Nevière, "Electromagnetic theory of diffraction in nonlinear optics and surface-enhanced nonlinear optical effects," Phys. Rev. B **28**, 1870–1885 (1983).
3. J. L. Coutaz, M. Nevière, E. Pic, and R. Reinisch, "Experi-

mental study of surface-enhanced second-harmonic generation on silver gratings," Phys. Rev. B **32**, 2227–2232 (1985).
4. M. Nevière, R. Reinisch, and D. Maystre, "Surface-enhanced second-harmonic generation at a silver grating: a numerical study," Phys. Rev. B **32**, 3634–3641 (1985).
5. M. Nevière, P. Vincent, D. Maystre, R. Reinisch, and J. Coutaz, "Differential theory for metallic gratings in nonlinear optics. Second-harmonic generation," J. Opt. Soc. Am. B **5**, 330–337 (1988).
6. H. J. Simon and Z. Chen, "Optical second-harmonic generation with grating-coupled surface plasmons from a quartz–silver–quartz grating structure," Phys. Rev. B **39**, 3077–3085 (1989).
7. X. D. Zhu, Th. Rasing, and Y. R. Shen, "Surface diffusion of CO on Ni(111) studied by diffraction of optical second-harmonic generation off a monolayer grating," Phys. Rev. Lett. **61**, 2883–2885 (1988).
8. G. A. Reider, M. Huemer, and A. J. Schmidt, "Surface second harmonic generation spectroscopy without interference of substrate contributions," Opt. Commun. **68**, 149–152 (1988).
9. T. Suzuki and T. F. Heinz, "Surface-harmonic diffraction from a monolayer grating," Opt. Lett. **14**, 1201–1203 (1989).
10. R. W. J. Hollering, Q. H. F. Vrehen, and G. Marowsky, "Angular dependence of optical second-harmonic generation from a monolayer grating," Opt. Commun. **78**, 387–392 (1990).
11. G. A. Reider, U. Höfer, and T. F. Heinz, "Surface diffusion of hydrogen on Si(111)7 × 7," Phys. Rev. Lett. **66**, 1994–1997 (1991).
12. X. Xiao, X. D. Zhu, W. Daum, and Y. R. Shen, "Optical second-harmonic diffraction study of anisotropic surface diffusion: CO on Ni(110)," Phys. Rev. B **46**, 9732–9743 (1992).
13. A. C. R. Pipino, G. R. Schatz, and R. P. Van Duyne, "Surface-enhanced second-harmonic diffraction: selective enhancement by spatial harmonics," Phys. Rev. B **49**, 8320–8330 (1994).
14. A. C. R. Pipino, R. P. Van Duyne, and G. C. Schatz, "Surface-enhanced second-harmonic diffraction: experimental investigation of selective enhancement," Phys. Rev. B **53**, 4162–4169 (1996).
15. M. Nevière, E. Popov, and R. Reinisch, "Electromagnetic resonances in linear and nonlinear optics: phenomenological study of grating behavior through the poles and zeros of the scattering operator," J. Opt. Soc. Am. A **12**, 513–523 (1995).
16. E. Popov, M. Nevière, G. Blau, and R. Reinisch, "Numerical optimization of grating-enhanced second-harmonic generation in optical waveguides," J. Opt. Soc. Am. B **12**, 2390–2397 (1995).
17. V. Berger, "Nonlinear photonic crystals," Phys. Rev. Lett. **81**, 4136–4139 (1998).
18. N. G. R. Broderick, G. W. Ross, H. L. Offerhaus, D. J. Richardson, and D. C. Hanna, "Hexagonally poled lithium niobate: a two-dimensional nonlinear photonic crystal," Phys. Rev. Lett. **84**, 4345–4348 (2000).
19. T. F. Krauss, R. M. De La Rue, and S. Brand, "Two-dimensional photonic-bandgap structures operating at near-infrared wavelengths," Nature **383**, 699–702 (1996).
20. For recent reviews see, e.g., C. M. Soukoulis, ed., *Photonic Crystals and Light Localization in the 21st Century*, Vol. 563 of NATO Science Series C: Mathematical and Physical Sciences (Kluwer, Dordrecht, The Netherlands, 2001).
21. D. Labilloy, H. Benisty, C. Weisbuch, T. F. Krauss, R. M. De La Rue, V. Bardinal, R. Houdré, U. Oesterle, D. Cassagne, and C. Jouanin, "Quantitative measurement of transmission, reflection, and diffraction of two-dimensional photonic band gap structures at near-infrared wavelengths," Phys. Rev. Lett. **79**, 4147–4150 (1997).
22. H. Benisty, C. Weisbuch, D. Labilloy, M. Rattier, C. J. M. Smith, T. F. Krauss, R. M. De La Rue, R. Houdré, U. Oesterle, C. Jouanin, and D. Cassagne, "Optical and confinement properties of two-dimensional photonic crystals," J. Lightwave Technol. **17**, 2063–2077 (1999).
23. M. Galli, M. Agio, L. C. Andreani, L. Atzeni, D. Bajoni, G. Guizzeti, L. Businaro, E. D. Fabrizio, F. Romanato, and A. Passaseo, "Optical properties and photonic bands of GaAs photonic crystal waveguides with a tilted square lattice," Eur. Phys. J. B **27**, 79–87 (2002).
24. V. N. Astratov, D. M. Whittaker, I. S. Culshaw, R. M. Stevenson, M. S. Skolnick, T. F. Krauss, and R. M. De La Rue, "Photonic band-structure effects in the reflectivity of periodically patterned waveguides," Phys. Rev. B **60**, R16255–R16258 (1999).
25. N. Bloembergen and P. S. Pershan, "Light waves at the boundary of nonlinear media," Phys. Rev. **128**, 606–622 (1962).
26. J. Ducuing and N. Bloembergen, "Observation of reflected light harmonics at the boundary of piezoelectric crystals," Phys. Rev. Lett. **10**, 474–476 (1963).
27. R. K. Chang, J. Ducuing, and N. Bloembergen, "Dispersion of the optical nonlinearity in semiconductors," Phys. Rev. Lett. **15**, 415–418 (1965).